Improvement and Validation of the Fluoroptic Temperature-Measurement Method

Arthur M. C. Janse, Xander A. de Jong, Wolter Prins, Wim P. M. van Swaaij
Dept. of Chemical Technology, Twente University, P.O. Box 217, 7500 AE Enschede, The Netherlands

The fluoroptic measurement method, recently developed by Wagenaar and coworkers to determine in a contactless manner the temperature of moving particles, has been improved. It now has a higher accuracy (approximately 5%) and can be used for particles that move at higher speeds. In addition, the technique has become much less labor-intensive. Validation has been realized by comparing experimentally determined heat-transfer coefficients for a cylinder in crossflow with predictions of several well-known correlations from the literature. A consistent deviation of less than 10% is observed. This comparison therefore shows the reliability of the fluoroptic measurement method.

Introduction

Knowledge of the external heat-transfer coefficient α of a particle is important for the design of process equipment in which the particle has to be processed. Examples of such processes are drying, calcination or roasting of solids, and the combustion, gasification, and pyrolysis of biomass and waste material. External heat-transfer coefficients can be determined from the combination of temperature change and heat-transfer exposure time. Several experimental techniques are available to determine the temperature of flowing particles. Wagenaar et al. (1994a) compiled an extensive survey and discussed measurements with thermocouples, particle collectors, two-color pyrometers, change in magnetic permeability of ferrites, liquid crystals, drying and sublimation of solids, and change in quantum yield of phosphors (fluoroptic measurement method). They demonstrated that this last method was best suited to determine the temperature of particles flowing with high speeds, and subsequently developed this novel, contactless technique further for application in the rotating cone reactor. A short introduction on the fluoroptic measurement method is given below.

Correspondence concerning this article should be addressed to W. Prins.
Present address of A. M. C. Janse: Gist-Brocades, P.O. Box 1, 2600 MA Delft, The Netherlands.

Principles of the Fluoroptic Technique

The utilization of phosphors constitutes the essence of this method. Upon illumination by UV light, they eventually show luminescence (emit visible radiation). On an atomic level, this is explained by absorption of light quanta, which can bring electrons from the ground state into an excited state (of a higher energy level with respect to the ground state). Subsequently, an "excited" electron can return to the ground state in two ways. First, a light quantum can be emitted: its energy is determined by the difference in energy levels between the ground state and the excited state. Second, the energy can be dispersed as vibration energy to the mother lattice, without emitting a quantum. This last route becomes gradually more important at higher temperatures, and is also indicated as thermal quenching. Consequently, the quantum efficiency, defined as the ratio of emitted and absorbed quanta (at a specific wavelength), will decrease at higher temperatures (Kröger, 1948; Blasse and Bril, 1970).

For a useful measurement method two phosphor types, which emit radiation in a different part of the spectrum after illumination, should be mixed. Only one of them should exhibit a temperature-dependent quantum yield in the considered temperature range. Wagenaar et al. (1994a) selected the following combination:

• Phosphor $BaMgAl_{10}O_{17}$: Eu (hereafter abbreviated as BAM)

• Phosphor $Sr_4Al_{14}O_{25}$: Eu (SAE)

where Eu stands for the rare metal europium.

The BAM phosphor (Philips type U716) has a light-intensity maximum at a wavelength of 488 nm (blue) and shows temperature-independent fluorescence (in the investigated temperature range), while the SAE phosphor (Philips type U 724) has a maximum at 447 nm (green) and exhibits a temperature-dependent quantum efficiency. At temperatures above 100°C thermal quenching of this phosphor occurs and the emitted radiation spectrum is dominated by the blue phosphor. At 250°C SAE is completely extinguished, so the temperature window in which measurements can be carried out with the BAM/SAE mixture is from 100 to 250°C. The emitted light is collected in a glass-fiber cable and divided in two spectral ranges by two optical filters: 400–490 nm and 500–700 nm. Both signals are amplified by photomultipliers, and the ratio of these two signals, which is a unique function of temperature, is determined. Thus, by using a calibration curve that relates each ratio to a specific temperature, the temperature of moving particles can be determined by measuring the blue/green ratio. The temperature-independent phosphor BAM is added to avoid dependency on the detected amount of fluorescent material. By measuring the ratio of two phosphors, which are contained in the same particle, instead of a quantum yield, all (unknown) effects influencing the total amount of detected photons are eliminated. Wagenaar remarks correctly that the fluoroptic measurement method shows some similarity with the two-color pyrometer measurement method (Jorgensen and Zuiderwyk, 1985). It has been checked that one of the dyes cannot excite the other. Therefore, the excitation spectra and emission spectra of the two phosphors are presented (see the Appendix).

A scheme of the required setup with the technical specification of its components is given in Wagenaar et al. (1994a); the main components are:

• A UV lamp. A high-pressure, direct-current, mercury arc lamp (type Ushio USH-205S) with an electrical dissipation of 200 W in the light bulb was applied.

• A quartz light guide. This cable is able to transmit the UV light with an overall efficiency of 30%.

• A filter at the end of the quartz cable that transmits the UV light and removes the visible light of the UV lamp. A Schott DUG 11 filter has been applied that transmits UV light in the wavelength range of 300–400 nm.

• Phosphors that are melted in lead–monosilicate glass ($PbO(SiO_2)_{1.03}$) to obtain particles of a specific size. The particle preparation procedure is discussed by Wagenaar et al. (1994a).

• A glass-fiber light guide (Dolan and Jenner) to collect the emitted radiation of the phosphors. This light guide was protected from UV-radiation with aid of an UV-filter (Balzer).

• Two bandfilters were used to separate the light emitted by the particles into two specific fractions:

(i) a Schott BSF Magenta bandfilter that transmits light in the 400–490-nm wavelength (blue light transmission)

(ii) a Schott KV500 bandfilter that transmits light in the 500–700–nm wavelength interval.

• Two photomultipliers (type Hamamatsu R928). These photomultipliers were able to amplify the incoming signal with a factor 10^7.

• Electronic amplification circuit, which is discussed extensively by Wagenaar et al. (1994a).

• A data-processing unit to determine the emitted light ratio.

• Several oculars to obtain coherent light bundles (UV light, visible light from the phosphors).

The old phosphor BAM/SAE mixture had several disadvantages (see the following section) that complicated the application. After a careful search, an improved combination could be selected consisting of: $Y_3Al_5O_{12}$:Ce(YAG), Philips type U720; $Sr_2P_2O_7$:Eu (SPE), Philips type U472.

The differences between the BAM/SAE and YAG/SPE phosphor mixture will be outlined first, after which the main characteristics of the new phosphor combination will be discussed.

Comparison of the Old and New Phosphor Combination

The BAM/SAE phosphor combination shows only one intensity maximum, while the intensity maxima of the two phosphors YAG and SPE are separate from each other in the radiation spectrum, which simplifies the detection and enhances the accuracy. Application of a double-peak spectrum, instead of an overlapping spectrum, has the distinct advantage that the amplifiers of both spectra can be optimized separately. Using the phosphor combination of Wagenaar et al. (1994a), the low quantum yield of the SAE phosphor could not be amplified very much because of the large BAM signal (that) partly overlapped the SAE signal. The intensity curves at 25°C are given in Figure 1 for both the old and new phosphor combination. They have been normalized to the maximal intensity, which is taken to be 100%.

The curve of the new phosphor combination shows two maxima: the first one belongs to SPE, the second one to YAG. The intensity maximum of YAG [at approximately 545 nm (563 nm according to the Philips Information Book (1990)],

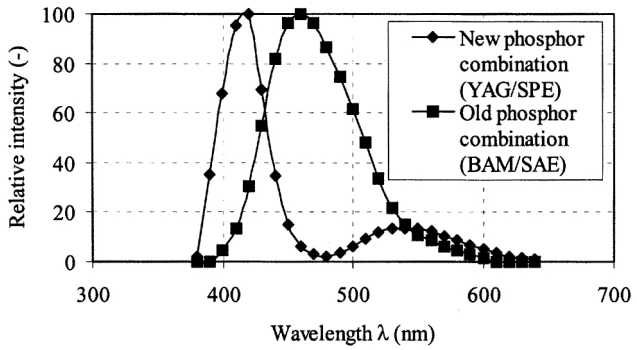

Figure 1. Intensity change as a function of the wavelength at 25°C for a mixture of equal amounts of phosphors.

which emits yellow light, is much lower than for SPE (at 418 nm), which emits blue light. This is caused by the difference in quantum efficiency (defined as the ratio of the number of quanta emitted by the phosphor and the number of quanta absorbed by the phosphor), which is 35% for YAG and 89% for SPE at room temperature (information book of Philips (1990)). To obtain equal quanta intensities at room temperature, YAG and SPE are mixed in the mass ratio, 3:1, for the production of fluorescent particles.

The YAG and SPE phosphors respond faster on illumination than do the BAM and SAE phosphors. The response time of the old combination could have been improved by heat treatment, but that would decrease the quantum efficiency (with an unacceptable low accuracy of the temperature determination as a logical consequence).

The BAM/SAE combination had to be calibrated after each measurement because the signal of the SAE phosphor becomes gradually weaker when repeatedly exposed to heat. This seriously delayed the experimental work. By this deactivation, the lifetime of the old combination was limited to a maximum of one month. The new combination has been used for several months, without any significant loss of quantum efficiency.

The operational temperature range is extended considerably with this new phosphor combination, namely, from 100–250°C (BAM/SAE) to 50–300°C (YAG/SPE). Above 300°C SPE is completely extinguished, below 50°C SPE responds too slowly on illumination with UV light.

Experimental Characterization of the New Phosphor Combination

Although the new phosphor combination is considerably improved, careful characterization is still needed to assure a good performance.

In the ideal case, every phosphor combination should respond instantaneously when the temperature changes and on illumination with UV light. Besides, the two phosphors should emit radiation in different wavelength regions, and the ratio of the light intensities should display a unique temperature dependency. Both phosphors must have a white color in the visible light part of the radiation spectrum to avoid absorption of specific wavelengths, which can be emitted by the other phosphor. Such a selective absorption would introduce dependency on the particle concentration. Finally, the quantum efficiency must be time independent and insensitive to heat treatments. Several tests have been carried out to assure that the new phosphor combination meets the requirements just specified. These tests are discussed below.

The rate at which the phosphors can follow an imposed temperature change has been determined in a screen heater reactor, as depicted in Figure 2a (Westerhout et al., 1996), while a view of the experimental setup is presented in Figure 2b. The reactor contains a wire mesh that is clasped between two electrodes. Glass particles containing the two phosphors, or pure phosphor particles, are put on the stainless-steel screen, above which the UV-light guide and probe for the collection of the emitted radiation are installed. The position of UV-light guide and probe are quite similar as applied in the rotation cone reactor, as is extensively discussed by Wagenaar et al. (1994a). At the start of an experiment a very high current (approximately 200 A) is conducted through the screen, which is therefore heated in a very short time.

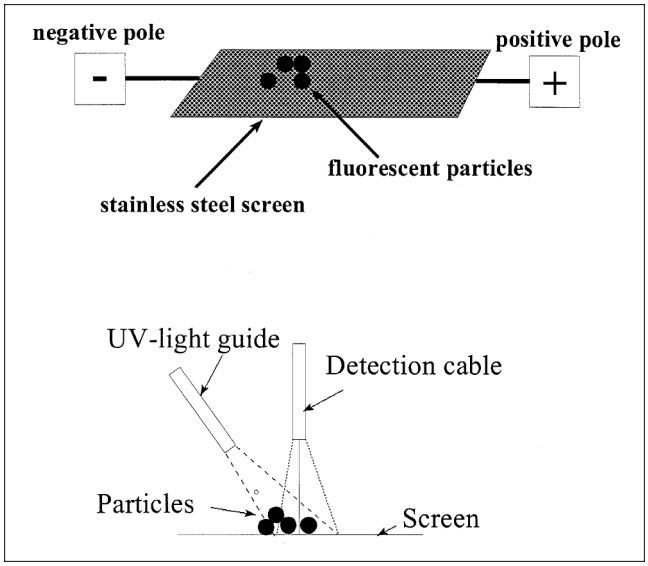

Figure 2. (a) screen heater reactor; (b) experimental setup.

An example of the result of such an experiment is given in Figure 3, which shows the relative (to the maximum value of the glass particles signal) intensity of the blue, temperature-dependent, SPE phosphor as a function of the time. In the beginning, the temperature of the phosphor is 20°C (maximal quantum intensity). At time zero the electric current is switched on and the screen in rapidly heated to 300°C. At this temperature level the SPE phosphor is almost completely extinguished. The figure shows an experiment for phosphor containing glass particles with a diameter of 80–120 μm and for pure phosphor (SPE) with a maximum diameter of 5 μm. The slope of the curve for the pure phosphor corresponds to a heating rate of approximately 10,000°C/s because

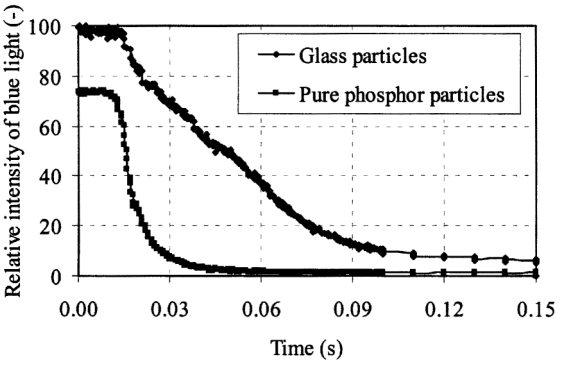

Figure 3. Screen-heater experiments to determine the response time on a temperature change from 20 to 300°C.

The delay of 10 ms at the beginning is the response time of the electrical equipment.

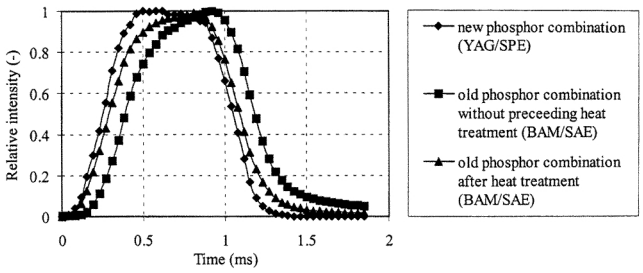

Figure 4. Dynamics of the BAM/SAE and YAG/SPE phosphors on illumination with UV radiation.

the temperature increases from 20°C to 300°C within 0.03 s. In the same way, the heating rate of the phosphor containing glass particles is deduced to be approximately 3,000°C/s.

The response rate on illumination has been measured by distributing fluorescent particles on a small heated plate (1 cm^2). A rotating disk is placed between the heated plate and the UV-light source, and a small hole in that disk is used to illuminate the particles frequently for a very short time (1 ms). Figure 4 shows the response for both the YAG/SPE and the BAM/SAE combination developed earlier. For the latter, two response curves are shown, one of them referring to a situation in which the phosphor had been preheated before the response measurement (12 h at 300°C). The new combination responds faster on a light pulse than the old phosphor combination, while for the latter a heat treatment appeared to be necessary to realize a sufficiently short response time on illumination (Wagenaar et al., 1994a). In relation to this subject, it has been verified that the emitted light intensity ratio of moving phosphor particles is equal to that of non-moving particles at constant temperature.

The intensity spectrum of the YAG/SPE phosphor combination has been determined at five different temperatures (Figure 5). At room temperature, the YAG phosphor has a maximum intensity at a wavelength of 545 nm, while the SPE phosphor has its maximum at 418 nm. It is clear from this picture that the two wavelength regions of emittance are at a sufficient distance from each other to allow a separate determination of the intensity for the two phosphors. This figure

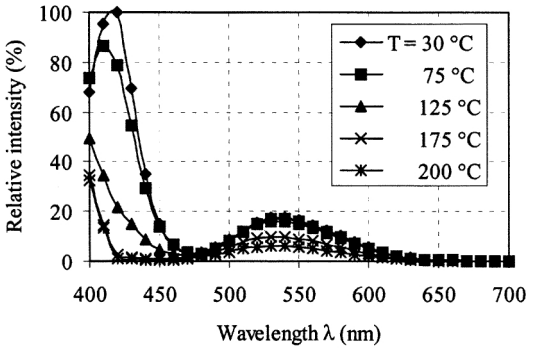

Figure 5. Intensity of the YAG and SPE as a function of wavelength for various temperatures (mass ratio 1:1).

also shows that both phosphors have a decreasing quantum efficiency at increasing temperatures. The relative light intensity decreased by a factor of 10 and 3 for SPE and YAG, respectively, when the temperature was increased from 30°C to 200°C. The emission spectra of the two phosphors at room temperature are shown separately in the Appendix (Philips Information Book, 1990).

It has been observed that the quantum yield did not change in time. During the 4-month experimental program, the calibration curve was verified each week, but this curve revealed no change in ratio during this time.

Finally, the deviation between three measurements is within 5%, which is the combined effect of the amplification of the signal and the calibration curve [which relates the blue/yellow ratio to a temperature (as discussed in paragraph 5)].

Solutions of Remaining Problems

The YAG/SPE phosphor combination also had some disadvantages. Special experiments revealed the following difficulties:

1. The angle under which the emitted light enters the light-conducting probe can affect the observed blue/yellow emitted light ratio.
2. The ratio is slightly dependent (10%) on the particle concentration.
3. The background can affect the ratio (also discussed by Wagenaar et al., 1994b).

1. Light is transported through a very thin glass fiber by reflection. Because of the large number of reflections, losses by absorption of the wall are unacceptable. When light enters the fiber at an angle higher than the so-called critical angle, part of the light bundle will be absorbed (Blasse and Bril, 1970). This is illustrated in Figure 6; the lefthand side (Figure 6a) shows a light bundle that is only partly reflected. In Figure 6b, light enters the fiber just at the critical angle, and part of it will be transmitted parallel to the surface. In Figure 6c, light enters the fiber at an angle lower than the critical angle and no loss of radiation occurs, because all the light is now reflected.

Because the critical angle is a function of the wavelength of the entering light, the measured light ratio is also a function of the entrance angle. In the experimental setup many particles at various positions are emitting light. It is therefore unavoidable that light from a wide range of angles will enter the probe fiber. This is shown in Figure 7, which includes the light conductor (or probe) and some particles emitting light from different positions.

Light entering the probe from a wide range of angles (coming from particles some distance to the side of the probe instead of from a position directly below it) results in a higher blue/yellow ratio than light from particles just below the probe (Figure 7). This can be explained by the fact that the critical angle ($\alpha_{critical}$, see Figure 6) depends on the wavelength of the incoming radiation. When the entrance angle of light is higher than the critical angle of yellow light, but lower than the critical angle of blue light, the intensity of the yellow light will decrease by *partial* reflection in the fiber. Because

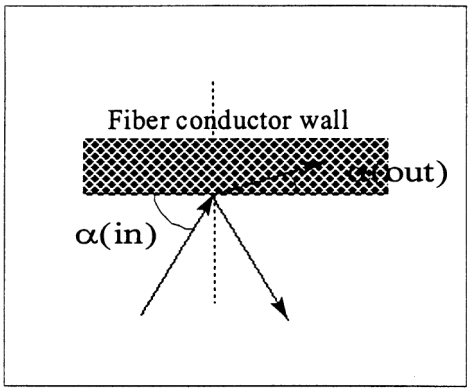

Figure 6. (a–c) Reflection and absorption of an entering light bundle.

the blue light does not suffer from a loss in intensity, the blue/yellow light ratio will increase.

To sufficiently reduce the problems mentioned earlier, a small black tube (or shaft) 2.5-cm long was attached to the top of the probe. This shaft, however, also results in a strong decrease in the observed relative light intensity of any radiation entering the probe at an angle of more than 20°. The effect of the shaft is further illustrated by Figures 8 and 9. Figure 8 shows the determined ratio as a function of the entrance angle for the situation with and without the shaft. The experiments were carried out by determining the blue/yellow ratio while moving the probe in a horizontal plane at a fixed vertical distance between the particles and probe. It seems that the black paper of the shaft selectively absorbs the blue component of the entering radiation, especially at high entrance angles ("more diffuse") of the incoming light. Therefore, to avoid the influence of this "more diffuse" light, it should be adsorbed as much as possible by the shaft. Figure 8 depicts the relative intensity of blue plus yellow light for the situation with and without a shaft. For the situation with a shaft, entrance angles of more than 20° do not influence the determined ratio because of the very low light intensity (see Figure 9), while without the shaft, angles of more than 30° still have a strong influence. To reduce the noise, especially at low signals, each data point has been measured many times (3–10). Each presented data point is the average of these measurements. The conclusion that the effect of diffuse incoming radiation is suppressed successfully by application of a shaft is therefore justified, although the total light intensity is reduced by approximately 30%. Because Wagenaar showed that the accuracy of the detection system is proportional to the inverse of the (square root) of the light intensity, it is

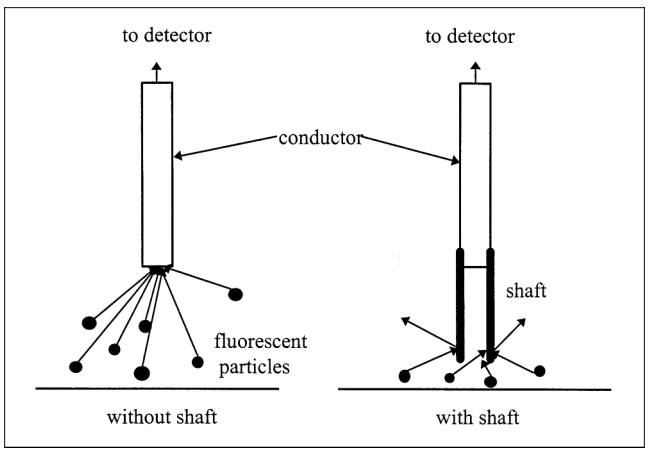

Figure 7. Experimental setup without (left) and with (right) shaft.

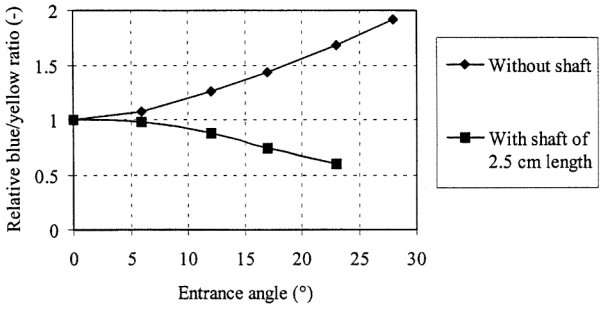

Figure 8. Angle dependency of the ratio.

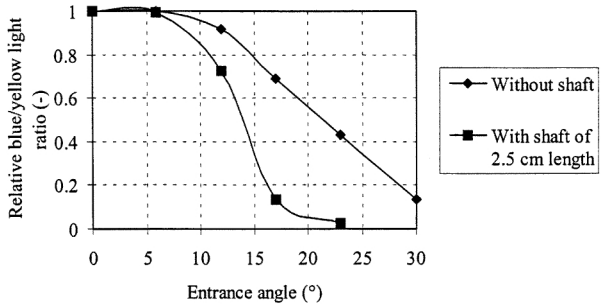

Figure 9. Relative intensity as a function of the entrance angle.

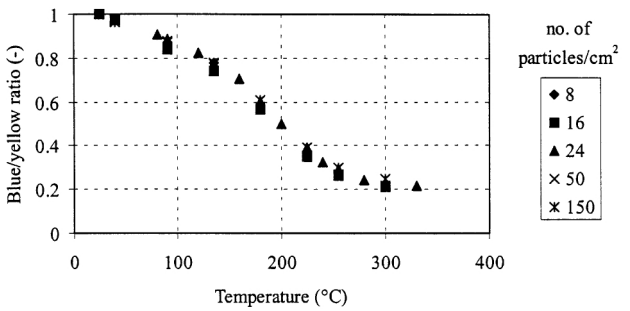

Figure 11. Stadartdized calibration curve.

unavoidable that the inaccuracy of the measurements will increase when using the shaft.

2. Unfortunately, experiments showed that the ratio of blue/yellow light is a function of the particle concentration. The old phosphor combination also suffered from this drawback, but the situation with the new mixture is more severe. The blue/yellow ratio increased up to 10% at constant temperature when the particle concentration was enlarged by a factor of 10, while the blue/yellow ratio of the old phosphor combination changed only 5%. Excitation of the YAG by the SPE phosphor is impossible, as has been verified by experimental work and information from the manufacturer [Philips Information Book (1990); see excitation spectra of the YAG and SPE in the Appendix]. It is therefore likely that the blue component of the white light of the SPE is partly affected as yellow light by the YAG. This assumption was indeed confirmed by illumination experiments with several filters. The color (nonwhiteness) of the phosphor constitutes a serious limitation of this technique, which unfortunately cannot be avoided. All types of phosphors that are commercially available in Europe (manufacturers Philips and Riedel de Haan) have been tested, but one could not be found that performed better.

The blue/yellow ratio must be related to the particle temperature by calibration. Therefore, a few particles were placed on a heated plate whose temperature could be varied. The so-called calibration curve was constructed by recording the blue/yellow ratio over the temperature range 20–300°C. However, because the particle concentration influenced the recorded blue/yellow ratio, the calibration curve was corrected for this effect by dividing the ratio at each temperature by the ratio at 25°C. Figure 10 shows the uncorrected calibration curves for a concentration of 8 particles (of 100 μm diameter) per cm^2, implying a distance of a few mm between the particles, to 150 particles per cm^2, whereby the particles were in contact with each other. Differences of more than 10% can be observed. Figure 11 shows the single normalized calibration curve, which is now almost independent of the particle concentration. The particle concentration dependency makes the method quite labor intensive, because each temperature measurement should be followed by a corresponding measurement at 25°C.

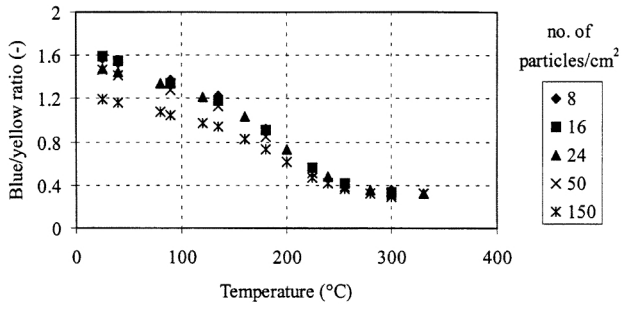

Figure 10. Unstandardized calibration curve.

3. The calibration curve was determined with a background of stainless steel and brass (which has a yellow color). The blue/yellow ratio is lower at all temperatures for the brass background if compared to the stainless-steel background. This is because brass reflects the yellow light of the YAG phosphor, but not the blue light of the SPE. Because the background of the calibration setup can have a substantial (negative) effect, this background should be of the same material as in the equipment used for the rotating-cone experiments (stainless steel in this work).

Validation of the Fluoroptic Measurement Method

Introduction

To validate the improved fluoroptic temperature measurement method, the heat-transfer rate to a cylinder in crossflow was examined. The direct external measurement of the cylinder temperature with a thermocouple is impossible without disturbing the flow profile. Therefore, heat-transfer coefficients, derived from a heating curve recorded by fluoroptic temperature measurement, were compared with values predicted by several correlations in the literature.

The coefficient of heat transfer to a cylinder, expressed as the nondimensional Nusselt number (Nu_c), is a function of the following dimensionless groups (Morgan, 1975):

$$Nu_c = Nu_c\left(Re,\, Gr,\, Pr,\, \frac{T_w}{T_b}\right), \qquad (1)$$

where Re represents the Reynolds number, Gr the Grashof number, Pr the Prandtl number, T_w the temperature of the cylinder surface, and T_b the temperature of the flowing medium. This relation can be simplified by realizing that Gr is only important when free convection is the dominating

heat-transfer mechanism. When the surface temperature does not deviate too much from the fluid temperature, Eq. 1 can be simplified to

$$Nu_c = CRe^m Pr^n. \tag{2}$$

Heat transfer to a cylinder by forced convection has been the subject of intensive research in the past. Applications vary from the design of (tube) heat exchangers on a large scale to the hot-wire anemometry on a small scale. Extensive reviews are published by Morgan (1975) and Zukauskas and Ziugzda (1985). These authors discuss the experimental methods applied and present an empirical correlation derived from their own work and the experimental results of others.

Most experiments have been carried out by fastening a cylinder at both sides in a fixed position in a wind tunnel. The cylinder is kept at a constant temperature electrically, and the external heat transfer can be calculated from the power input to achieve this constant temperature. The following difficulties (Morgan, 1975; Zukauskas and Ziugzda, 1985) are responsible for the differences in the various correlations in the literature describing the same heat-transfer phenomenon:

- Blockage of the free space for the gas flow by the cylinder in relatively narrow channels.
- Difference in turbulence level (even though *Re* may be equal).
- Difference in thermal driving force. By the strong influence of the temperature on the viscosity of the gas, the flow pattern around the cylindrical surface can be changed dramatically by a moderate change in temperature.
- Loss of heat by conduction to the clasps (in the case of steady-state measurements).
- Disturbance of the flow pattern by the measurement equipment.
- Different media.

Experimental studies

An experimental setup was designed, while trying to avoid the problems just listed as much as possible. It is sketched in Figure 12 and roughly consists of a heater section, and in front of it, a cylinder fixed inside a turnable holder. The diameter of the cylinder is 1.08 mm, and its total length is 4 cm. Gas enters the inlet of the 80-cm-long heater at the left side.

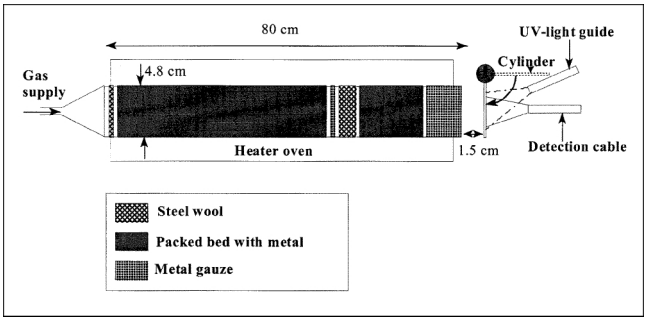

Figure 12. Setup of the cylinder in crossflow.

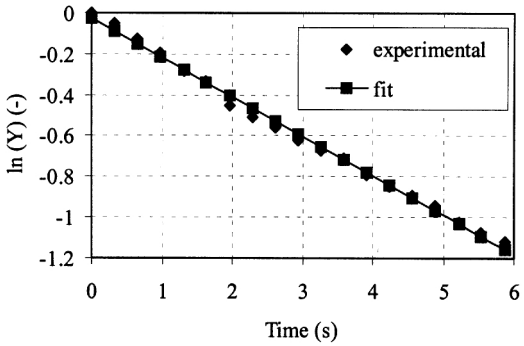

Figure 13. Typical plot of the dimensionless driving force *Y* (Eq. 4) against time *t* for heating of a cylinder in crossflow.

The gas flow is controlled by a rotameter, which is calibrated at cold flow conditions by a hot-wire anemometer that is located just in front of the cylinder. For the heat-transfer measurements, the gas velocity was varied from 1.5 to 5 m/s [41 $< Re <$ 135 (air, 300°C)]. The cylinder is attached at one side with a thermally isolated holder. At the start of an experiment, the oven is heated to the desired temperature. Afterward, the cold cylinder is placed in the gas flow outlet and heated within a few seconds to the gas-phase temperature. By locating the UV-light conductor and the probe just above the cylinder, the cylinder's temperature increase can be followed in time.

As with the sample particles of the problem-solution section, the cylinder is prepared again by sintering a mixture of lead monosilicate glass and two phosphors in a glass tube at a temperature of 600°C. Because the material shrinks during cooling, the cylinder can be removed easily from the tube. In this way, a cylinder with a very smooth surface is obtained.

It can be derived from a simple energy balance that the temperature increase of the cylinder in time is given by (assuming a constant heat-transfer coefficient)

$$\ln(Y) = \frac{4\alpha}{\rho c_p} t. \tag{3}$$

The dimensionless thermally driving force Y is defined as

$$Y = \frac{T_c - T_g}{T_0 - T_g}, \tag{4}$$

in which T_0 represents the initial (room) temperature. When $\ln(Y)$ is plotted against the time t, the slope of the straight line should be equal to $4\alpha/\rho c_p$. An example of the experimental results is presented in Figure 13.

A slight variation in the thermal driving force with a frequency on the order of 1/s is notable. This effect, which could be detected in every measurement, is probably caused by the cooling system of the UV light. The UV lamp is equipped with a filter to remove all the visible radiation. This filter is cooled with water to avoid excessive filter temperatures.

Sometimes small air bubbles are captured, and this change of medium in front of the UV light can give rise to a small variation in the determined blue/yellow ratio.

Disturbing phenomena

It has been verified that the following phenomena could not disturb the experiments:

1. Temperature gradients inside the cylinder in the radial direction.
2. Temperature gradients inside the cylinder in the axial direction
3. Radial temperature and velocity gradients in the gas phase near the cylinder surface
4. Turbulence of the gas flow just in front of the cylinder
5. Magnitude of the thermal driving force
6. Radiation and free convection
7. Roughness of the material
8. Effect of the finite length of the cylinder.

1. The relative influence of internal conduction is reflected by the value of the Biot number *Bi* (defined as $\alpha r/\lambda_s$). It represents the ratio of the heat-transfer resistance inside the cylinder (in the radial direction) and in the film surrounding the cylinder. If *Bi* is smaller than 0.3, then the influence of internal conduction on the total heat-transfer process can be neglected (Wagenaar, 1994b). The Biot number is coupled to the Nusselt number by

$$Bi = \frac{1}{2} Nu \frac{\lambda g}{\lambda_s}. \tag{5}$$

Therefore, with $\lambda_g = 0.05$ (at 300°C) and $\lambda_s = 0.5$ $W \cdot m^{-1} \cdot K^{-1}$ (lead monosilicate glass), a *Bi* number of 0.3 corresponds to a *Nu* number of approximately 6. In the present situation, the *Nu* number has an upper limit of 6 if the radial temperature gradients are to be avoided.

2. The amount of heat that is conducted through the cylinder in the axial direction $\phi_{h,\,ax}$ is estimated to be

$$\phi_{h,ax} = \frac{\lambda_s F_c \Delta T}{L_c} = 9.8 * 10^{-6} \Delta T. \tag{6}$$

In this equation, F_c represents the cross-sectional surface of the cylinder. The amount of heat that can be transferred through the stagnant gas film surrounding the cylinder $\phi_{h,\,r}$ is as follows:

$$\phi_{h,r} = \alpha A_c \Delta T = 19 \times 10^{-2} \Delta T, \tag{7}$$

in which A_c now represents the total external cylinder surface. In Eq. 5, a typical value for α of 150 $W \cdot m^{-2} \cdot K^{-1}$ is used. It appears that heat transfer from the gas to the cylinder is three orders of magnitude higher than the axial conduction of heat inside the cylinder.

3. The temperature and velocity field around the gas outlet of the tube have been mapped by using a thin thermocouple and a hot-wire anemometer, respectively. The gas bulk variations in temperature and velocity remain below 2% for all experimental conditions. Apparently, the metal gauze is able to successfully smooth the flow profile.

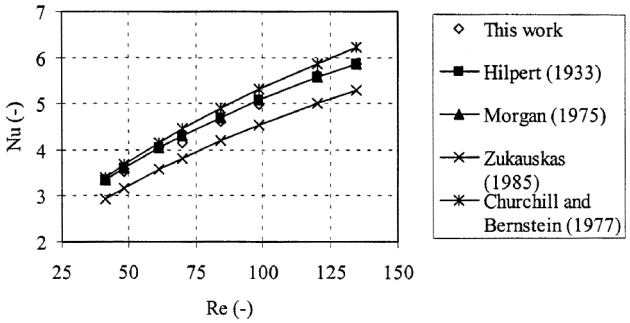

Figure 14. Experimentally determined vs. predicted *Nu* numbers for a crossflow cylinder in air at 300°C.

4. The degree of turbulence is expressed in the so-called turbulence number (*Tu*, unit: %), which is defined as the ratio of the variation in the gas velocity and the average gas velocity. By mapping the flow field at the same distance from the heater outlet as the cylinder with a hot-wire anemometer, it was observed that the *Tu* number in this work was limited to at most 2%. Zukauskas and Ziugzda (1985) remark that an increase in the *Tu* number from 1.2% to 15% is required to increase the heat transfer from 35% to 38% (in the subcritical range of *Re*, without a turbulent boundary layer).

5. The magnitude of the thermal driving force is normally expressed in the literature as the temperature loading (ratio of cylinder and gas-phase temperature). Two gas-phase temperatures have been applied to determine the effect of the difference in thermal driving force. No effect could be observed by changing the gas-phase temperature from 200°C to 300°C (compare Figures 14 and 15).

6. Because of the relatively small cylinder diameter and the completely free outflow of the gas, this effect could be neglected.

7. A very smooth surface was obtained by means of the applied sintering method used to prepare the cylinder. Any influence of surface roughness is therefore assumed to be absent.

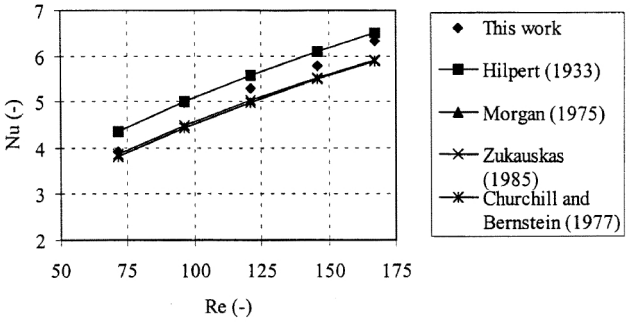

Figure 15. Experimentally determined vs. predicted *Nu* number for a crossflow cylinder in air at 200°C.

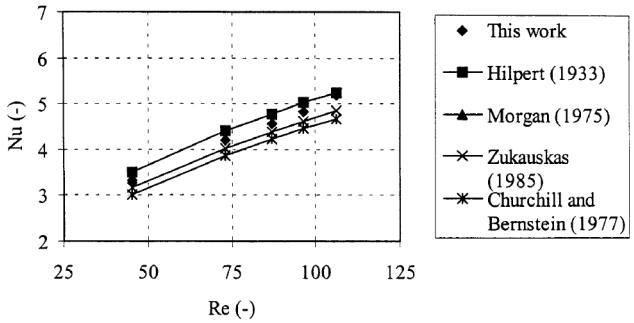

Figure 16. Experimentally determined vs. predicted *Nu* number for a crossflow cylinder in CO_2 at 300°C.

8. Quarmby and Al-Fakhri (1980) have shown that when the ratio of length and diameter (also known as the respect ratio) of the cylinder is more than 4, its effect can be neglected (in this work the aspect ratio equals 40).

Results of measurements

Three series of experiments have been carried out in which the *Nu* number was determined as a function of the corresponding *Re* number. The first two series at 200 and 300°C were meant to establish the influence of the size of the thermal driving force (or temperature loading factor). In the third series, CO_2 instead of air was used as gas phase (at 300°C) to determine the influence of the fluid type. The observed heat-transfer coefficients were compared with the predictions of several correlations in the literature (Hilpert, 1933; Morgan, 1975; Churchill and Bernstein, 1977; Zukauskas and Ziugzda, 1985). Figures 14–16 represent the result of this comparison. They reveal that the difference between the experimental curve and the average of the various correlations in the literature is always less than 10% for all three series of experiments.

Apparently, the conclusion is justified that the fluoroptic technique is adequate in determining the correct temperature of fluorescent particles as far as concerns the influences of (the size of) the driving force and the type of fluid.

Conclusions

The fluoroptic temperature measurement method has been improved with respect to the earlier work of Wagenaar (1994a) in such a way that it can be applied with higher accuracy (approximately 5%). Also, the new method is less labor-intensive. This measurement technique has been validated by comparing the coefficient of heat transfer to a cylinder in crossflow with predictions by various correlations in the literature. The result was quite satisfactory (the deviation was less than 10%), the contactless method of temperature measuring appears to be sufficiently reliable.

Acknowledgments

This investigation was supported by the CEC-AIR program (AIR-contract CT93-0889). We also acknowledge J. Nijmeijer, J. Waanders, and G. Schorfaar for their assistance in the experimental work.

Notation

C = constant
c_p = heat capacity, J/kg·K
d = diameter, m
g = gravity acceleration, m/s^2
L = length, m
m = mass, kg
r = radius, m
rt = blue/yellow or green/blue ratio
u = mean (gas-phase) velocity in direction of flow, m/s
u' = velocity fluctuation in direction of flow, m/s
v = (particle) velocity, m/s

Greek letters

γ = bulk expansion coefficient, K^{-1}
η = dynamic viscosity, Pas
λ = heat conductivity coefficient; wavelength, W/m/K; m
ν = kinematic viscosity, m^2/s
ρ = density, kg/m^3

Subscripts and Superscripts

b = bulk
c = cylinder
f = film
g = gas or air
m = constant
n = constant
p = particle
r = radial direction
s = solid phase

Literature Cited

Blasse, G.,and A. Bril, "Characteristic Luminescence," *Philips Tech. Rev.* **31**, 304 (1970).
Churchill, S. W., and M. Bernstein, "A Correlating Equation for Forced Convection from Gasses and Liquids to a Circular Cylinder in Cross Flow," *J. Heat Transfer*, **99**, 300 (1977).
Hilpert, R., "Warmeabgabe von geheizten Drathen und Rohren im Luftstrom," *Forsch. Ingenieurw.*, **4**, 215 (1933).
Jorgensen, F. R. A., and M. Zuiderwyk, "Two-Colour Pyrometer Measurement of the Temperature of Individual Combusting Particles," *J. Phys. E., Sci. Instrum.*, **18**, 486 (1985).
Kröger, F. A., *Some Aspects of Luminescence of Solids*, Elsevier, New York (1948).
Morgan, V. T., "The Overall Convective Heat Transfer from Smooth Circular Cylinders," *Adv. Heat Transfer*, **11**, 199 (1975).
Philips Information Book on Phosphors, Philips Phosphors, Philips, Eindhoven (1990).
Quarmby, A., and A. A. M. Al-Fakhri, "Effect of Finite Length on Forced Convection Heat Transfer from Cylinders," *Int. J. Heat Mass Transfer*, **23**, 463 (1980).
Wagenaar, B. M., R. Meijer, J. A. M. Kuipers, and W. P. M. van Swaaij, "A Novel Method for Noncontact Measurement of Particle Temperatures," *AIChE J.*, **41**, 773 (1994a).
Wagenaar, B. M, R. Meijer, J. A. M. Kuipers, and W. P. M. van Swaaij, "Fluoroptic Measurements of the Local Heat Transfer Coefficient Inside the Rotating Cone Reactor," *Chem. Eng. Sci.*, **49**, 773 (1994b).
Westerhout, R. W. J., R. H. P. Balk, R. Meijer, J. A. M. Kuipers, and W. P. M. van Swaaij, "Measurement and Modelling of High Temperature Pyrolysis Kinetics of PE and PP—Application of a Novel Screen Heater with a Gas Sweep," *Chem. Eng. Sci.*.
Zukauskas, A., and J. Ziugzda, *Heat Transfer of a Cylinder in Crossflow*, Hemisphere, Washington, DC (1985).

Appendix

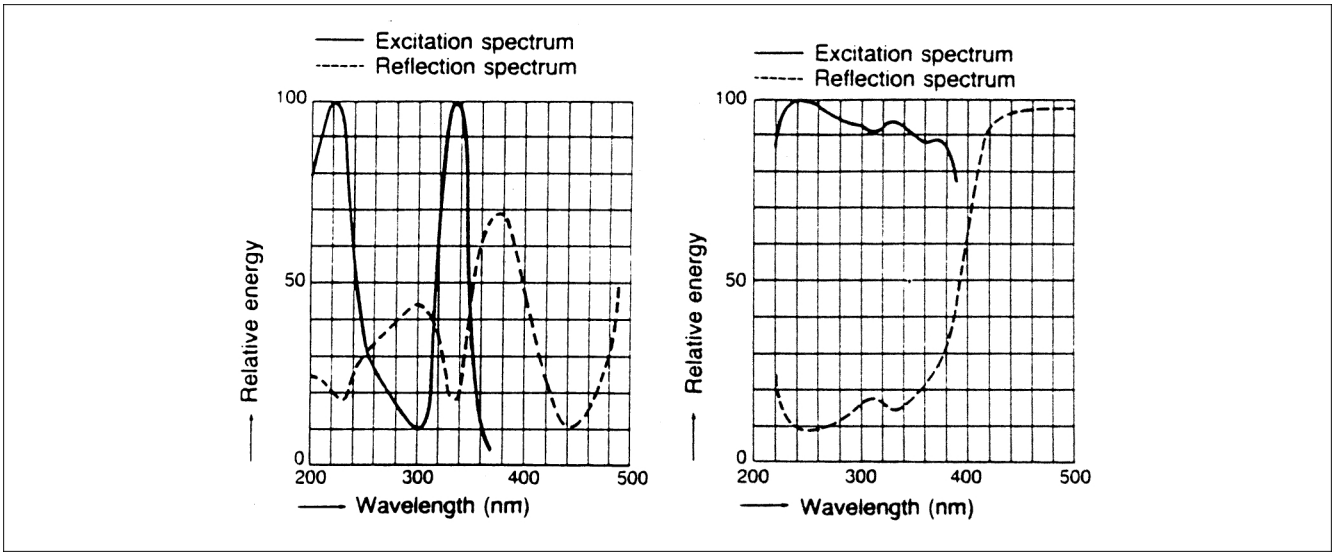

Figure A1. Excitation and reflection spectra of the YAG (left side) and the SPE phosphor (right side).

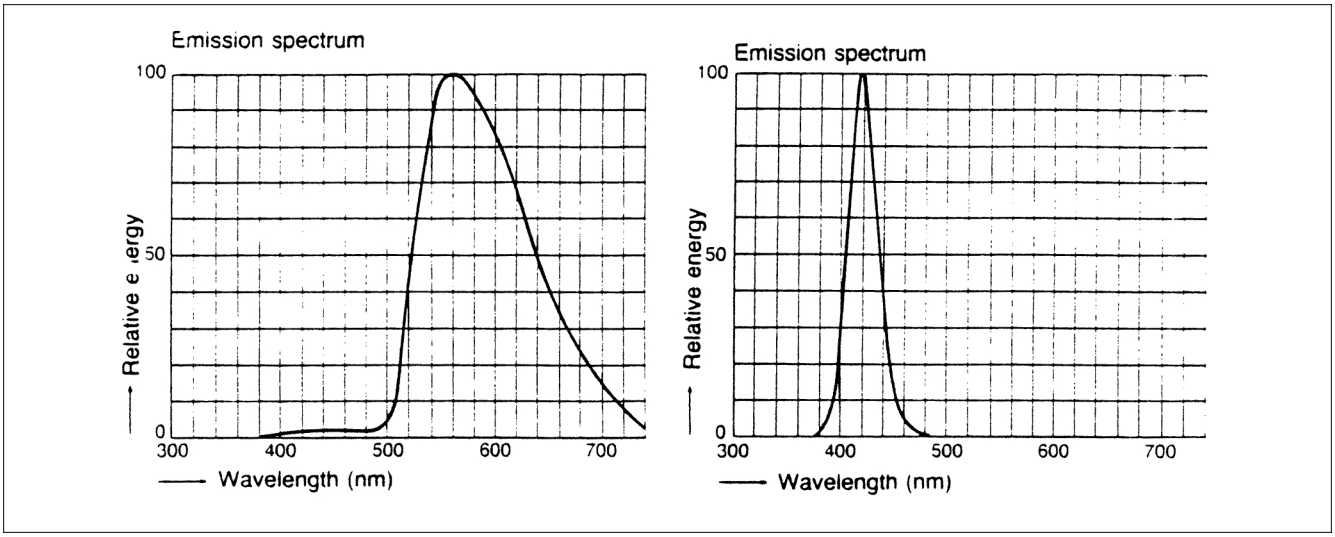

Figure A2. Emission spectra of the YAG (left side) and SPE phosphor (right side).

Manuscript received Nov. 9, 1998, and revision received Apr. 26, 1999.